The magnetization process and coercivity in random anisotropy systems

1995 J. Phys.: Condens. Matter 7 3301

(http://iopscience.iop.org/0953-8984/7/17/013)

J. Phys.: Condens. Matter 7 (1995) 3301–3313. Printed in the UK

The magnetization process and coercivity in random anisotropy systems

R Ribas†, B Dieny‡, B Barbara§ and A Labrata†

† Departament de Física Fonamental, Universitat de Barcelona, Avenida Diagonal 647, 08028 Barcelona, Spain

‡ Laboratoire de Métallurgie Physique, CENG, DRFMC/SP2M, 38054 Grenoble, France

§ Laboratoire Louis Néel, CNRS, BP 166, 38042, Grenoble Cédex 9, France

Received 15 December 1994

Abstract. A numerical simulation of a two-dimensional XY model has been carried out to study the thermal behaviour of the magnetization process and the variation of the coercive field as a function of the random anisotropy amplitude. The existence of two different magnetic regimes is evidenced: a low-anisotropy regime, which is characterized at zero temperature by a power law increase of the coercive field as the anisotropy amplitude increases, and a regime for anisotropy values higher than $D/zJ = 0.5$, for which the system behaves as an assembly of quasi-independent clusters of two or three atoms. In this regime, the coercive field increases linearly with the anisotropy strength. The numerical estimates of the power law exponent are in good agreement with the heuristic predictions of Imry and Ma. The domain wall motion and the spin configuration for the two anisotropy regimes have also been studied, pointing out the differences in the pinning process between both regimes. The thermal dependence of the coercive field has been obtained and fitted to an exponential law.

1. Introduction

In the last 20 years considerable effort has been devoted to the study of the magnetic properties of amorphous alloys, such as rare earth–transition metal alloys [1]. This interest was motivated by the anomalous magnetic properties observed experimentally in these alloys, such as the strong thermal and magnetic irreversibility, the absence of long-range order, the huge coercive fields observed at low temperature [2], and the existence of long relaxation times as in glasses [3]. All these facts are related to the high degree of ground state degeneracy and the existence of a large number of metastable states. Moreover, these facts are due to the microscopic disorder that has a determining influence on the magnetic behaviour observed for these materials. In particular, the presence of rare earth atoms plays an important role [4] in these alloys due to the single-ion anisotropy and crystal-field effects, which are very important for rare earth atoms. The spin–orbit coupling and the exchange interaction among the atoms of the alloy propagate the effect of the single-ion anisotropy from the rare earth atoms to the transition metal atoms, inducing a local easy axis of magnetization that varies from atom to atom through the crystal.

Since the study of the magnetic behaviour of $TbFe_2$ amorphous alloys by Rhyne *et al* [2] in 1974, increasing effort has been devoted to the understanding of the experimental results. In 1973, Harris and coworkers [5] proposed a model that gathered the main features of the experimental systems. This model is known as the HPZ model, and has been extensively studied using several techniques. The mean-field calculations performed by Harris *et al* [6]

0953-8984/95/173301+13$19.50

showed that this model can exhibit long-range order in three dimensions for low values of the random anisotropy. Later on, Imry and Ma [7] showed that the ferromagnetic phase was unstable in less than four dimensions. Finally, Aharony and Pytte [8] obtained the magnetic equation of state for the random anisotropy systems theoretically, which definitely confirmed the absence of long-range order from these systems and introduced a new method for analysing the experimental data.

The high coercive fields observed at low temperature have also attracted great attention. Callen *et al* [9] studied the dependence of the coercive field on the anisotropy strength at 0 K using mean-field techniques. Their results predicted a linear increase in the coercive field in the high-anisotropy limit. Later, Alben *et al* [10] studied the dependence of the coercive field on the anisotropy amplitude at zero temperature by numerical simulation. Their results showed a discrepancy with the previous results of Callen *et al* [9] in the high-anisotropy limit, where the coercive field reached a saturation value close to the exchange field J/μ_B. Patterson *et al* [11] studied the coercive field dependence using the local mean-field approach, which confirmed the previous results of Callen *et al* [9] at zero temperature, and they suggested that the discrepancy observed in the high-anisotropy limit could be due to the metastability and the irreversibility of these systems. Recently, Saslow and Koon [12] used numerical simulation to study the behaviour of a 3D random anisotropy system at zero temperature. Their results, showing the dependence of the coercive field on the ratio D/J at zero temperature, agreed with the previous results of Alben *et al* [10] in the low- and intermediate-anisotropy regions, but they did not reproduce the maximum of the coercive field observed by Alben *et al* in the high-anisotropy regime. Instead of this maximum, Saslow and Koon [12] obtained a saturation of the coercive field at a value close to $1.3J$. They suggest that this difference may be due to the lack of convergence of the numerical simulations performed by Alben *et al*.

The thermal behaviour of the coercive field has also been studied by different methods. On the one hand, experimental data obtained by Read *et al* [13], in FeZr amorphous alloys, and by Buschow and Kraan [14] in $Dy_{60}Fe_{40}$, suggest an exponential law for the coercive field as a function of temperature. Recently, Arnaudas *et al* [15] also obtained an exponential decrease in the coercive field of $(Gd_{1-x}Tb_x)_2Cu$ compounds, and related this behaviour to a change in the nature of the thermally activated processes governing the low-temperature magnetic properties. On the other hand, the numerical simulations performed by Jayaprakash and Kirkpatrick [16] and Denholm and Sluckin [17], and the theoretical calculations performed by Cresswell and Paul [18], showed a dependence of the coercive field on the temperature, which was qualitatively similar to an exponential decay, although no explicit attempt was made to fit the numerical data to an exponential law.

The coercive field is strongly related to the magnetization process (i.e. the domain wall motion and domain size distribution) and to the activation volumes of the system [19]. The study of the spin configurations of the system as the field is changed allows us to study the domain wall motion and helps in the understanding of the coercive field behaviour. In this direction, Chudnovsky *et al* [20] performed a theoretical study of the 2D and 3D amorphous magnets with random anisotropy. As a result, these authors pointed out the existence of two phases depending on the magnetic field strength. The low-field phase, called a correlated spin glass (CSG), is characterized by large magnetic domains distributed throughout the sample. In the high-field regime, close to saturation, the spins are approximately oriented in the field direction and the phase is called a ferromagnet with a wandering axis (FWA). Later, Dieny and Barbara [21] studied the existence and influence of topological defects in the 2D XY model with random anisotropy. Their results revealed the existence of various topological defects that influence the magnetization process.

The aim of this article is to study the magnetization process of a 2D XY model with random anisotropy to determine the dependence of the coercive field on the anisotropy strength at zero temperature, and the thermal behaviour of the coercive field for different anisotropy strengths. These results are useful to verify the exponential decay observed experimentally, and to give some insights for a better understanding of the activation mechanisms at low temperature. To achieve these goals, a deeper knowledge of the microscopic behaviour of the system is needed. For that purpose, numerical simulation is a valuable tool since it allows us to determine the magnetization of the system on the microscopic scale and study its evolution as the external parameters are changed.

This article is organized as follows. In section 2, we describe the model and discuss the numerical methods used in the simulation. In section 3 we analyse the spin configurations and the domain wall motion. In section 4, the coercive field dependence on anisotropy strength at zero temperature is determined. Finally, in section 5, the thermal behaviour of the coercive field is analysed.

2. Computational details

In this section the numerical methods and the system geometry are described. The system consists of a rectangular lattice with L_x spins along the longitudinal direction and $L_y < L_x$ spins in the transverse direction. The numerical values are $L_x = 100$ and $L_y = 10$. At each of the lattice points, a two-component unit vector spin, $\boldsymbol{S}_i$, is attached, which forms an angle θ_i with the longitudinal axis. This geometry is the most suitable for the visualization of the domains and the domain wall motion along the longitudinal direction. Free boundary conditions were imposed in both longitudinal and transverse directions, to avoid the formation of vortices in the system. These vortices, observed by Dieny and Barbara [21], could modify the magnetization process due to the correlations induced between spins on opposite sides of the system.

The energy of a random anisotropy system given by the HPZ model [5] is written

$$E = -J \sum_{\langle i,j \rangle} \boldsymbol{S}_i \cdot \boldsymbol{S}_j - D \sum_i (\boldsymbol{n}_i \cdot \boldsymbol{S}_i)^2 - g\mu \boldsymbol{H} \sum_i \boldsymbol{S}_i \tag{1}$$

where the first term is the exchange energy and the summation is extended over the nearest neighbours of the i spin. The second term is the random anisotropy contribution, where D is the anisotropy constant and $\boldsymbol{n}_i$ is the random anisotropy axis. The last term is associated with the external magnetic field $\boldsymbol{H}$; g is the gyromagnetic constant and μ is the magnetic moment of the spin.

It is worth distinguishing between two kinds of numerical simulation: the zero-temperature simulations, in which there is no thermal activation, and finite-temperature simulations, in which thermal activation is present. At zero temperature, the spins of the system should be in a local energy minimum. When the magnetic field is applied, the spin orientation changes to a new one corresponding to the nearest local energy minimum. However, the evolution towards the nearest minimum is such that there is no local energy increase since no activation occurs at 0 K. To take this fact into account, a steepest-decent algorithm [22] was used. This algorithm minimizes the local energy of each of the spins of the system by modifying the spin direction in such a way that the local energy decreases step by step along the direction of the energy gradient. If, for a given step, the local energy increases, the step size is reduced until energy decreases again. The process continues until

the sum (over the whole lattice) of the angular differences between successive configurations is smaller than the given tolerance. As a result, the total energy decreases and the system reaches an equilibrium state, characterized by a negligible change in the total energy. At this point, the magnetization and the total energy are calculated.

On the other hand, in the simulations at finite temperature, thermal activation takes place, which allows the energy barriers to be overcome. To take the thermal activation into account, the classical Monte Carlo method [23] was used. In this case the spin changes that involve an energy increase, ΔE, are accepted with the Boltzmann probability $\exp(-\Delta E/k_B T)$, where k_B is the Boltzmann constant and T is the absolute temperature.

For the simulations of the domain wall motion, the spins in the first column were fixed, parallel to the magnetic field direction, and the rest of the spins were opposite to the field direction and free to move as the field was changed. In this way, at zero magnetic field, there is a domain wall in the neighbourhood of the first column. As the magnetic field is increased, the domain wall moves. This motion can be visualized by keeping track of the spins' configurations. On the other hand, there were no fixed spins in the simulations of the coercive field behaviour. During all the simulations, the spins were selected in a random way to avoid correlations between successive configurations. The constants J and μ were chosen to simulate a typical ferromagnetic amorphous alloy [1] with $J = 1.035\ 10^{-15}$ erg and $\mu = 2$ Bohr magnetons. The ratio D/zJ of the anisotropy energy, D, to the exchange energy, zJ, was varied between 0.1 and 2. The magnetic field H was applied in the transverse direction (i.e. perpendicular to the longest dimension L_x of the system), which we will call the Y direction.

3. Spin configurations and domain wall motion

In this section, the equilibrium spin configuration and the domain wall motion are analysed. The equilibrium spin configurations at zero magnetic field are represented in figure 1 for different values of the anisotropy ratio. In this figure, only a part of the spin configuration is represented at zero field for small anisotropy ($D/zJ = 0.1$, figure 1(a)), intermediate anisotropy ($D/zJ = 0.5$, figure 1(b)) and high anisotropy ($D/zJ = 2$, figure 1(c)). The thick arrow indicates the direction in which the magnetic field will be applied. As seen from figure 1(a), in the low-anisotropy regime ($D/zJ = 0.1$), there is a high degree of order in the system, which is only disturbed in the neighbourhood of the artificially induced domain wall (i.e. close to the first column of spins). However, in the high-anisotropy region (between $D/zJ = 0.5$ and $D/zJ = 2$, figure 1(b) and (c)), the system splits into small clusters (with a characteristic length of two or three atomic distances). This behaviour has also been found by Chudnovsky *et al* [20] using phenomenological arguments based on the continuous energy density functional. The low-anisotropy limit, in which the system splits into large domains, was called a correlated spin glass [20].

To provide a better view of the magnetization process in these systems and in particular of the domain wall motion, the equilibrium spin configurations for different magnetic fields were recorded and the magnetization profile was calculated. This profile is calculated by averaging the component of the spin parallel to the field, S_y, in each column of the system (for each value of x). The results are shown in figure 2.

In the low-anisotropy case (figure 2(a)) at $H = 150$ Oe the magnetization remains similar to the zero-field situation, plotted in figure 1(a). When the field is increased, the magnetization starts to reverse. This occurs as a result of two competing processes:

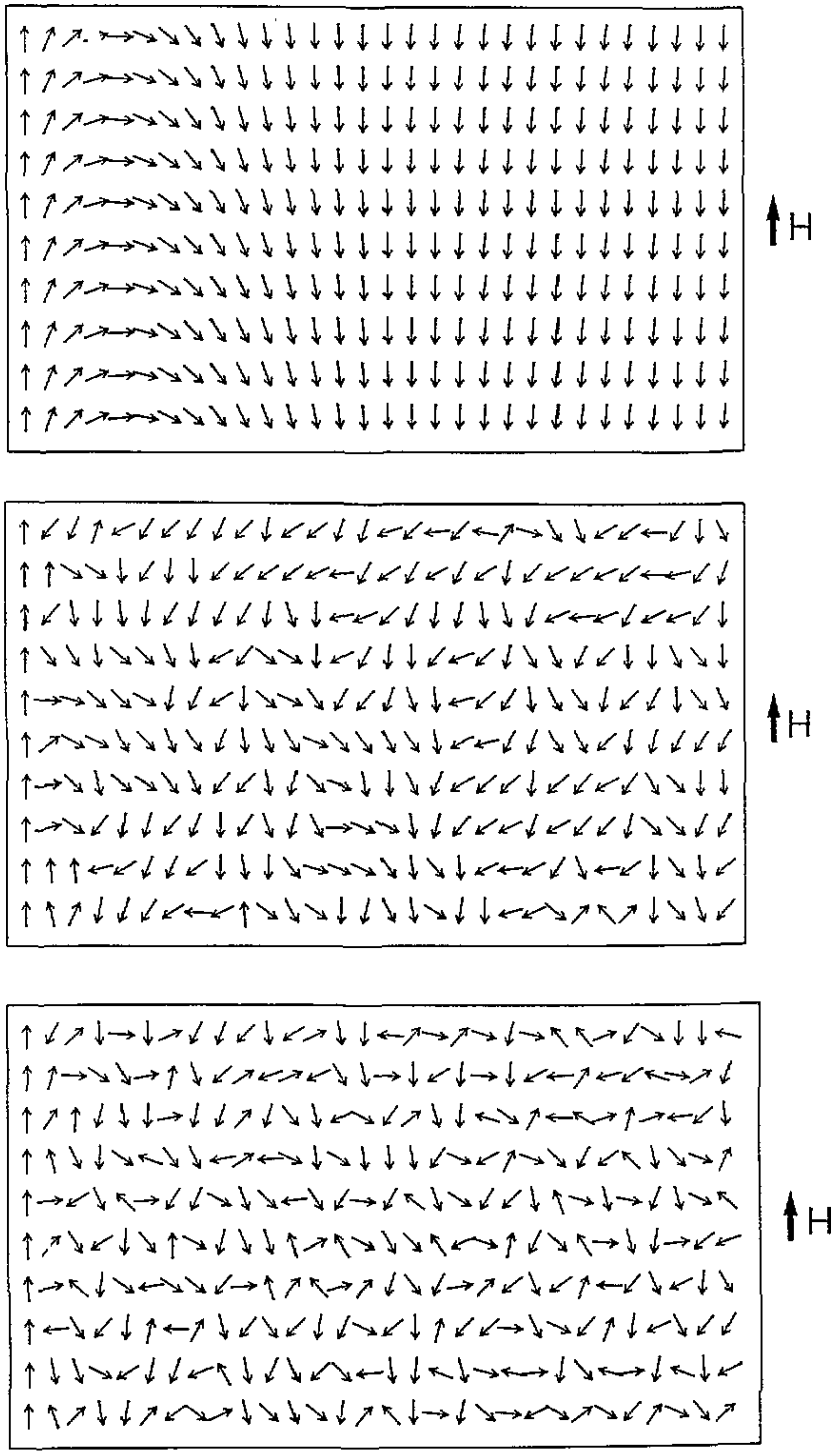

Figure 1. (*a*) Part of the equilibrium spin configuration at low anisotropy ($D/zJ = 0.1$) and zero field. The magnetic field is applied in the direction given by the thick arrow. (*b*) The same as (*a*) for $D/zJ = 0.5$. The magnetization is broken into small clusters. (*c*) The same as (*a*) for $D/zJ = 2$. The magnetization is broken into very small clusters of two or three spins.

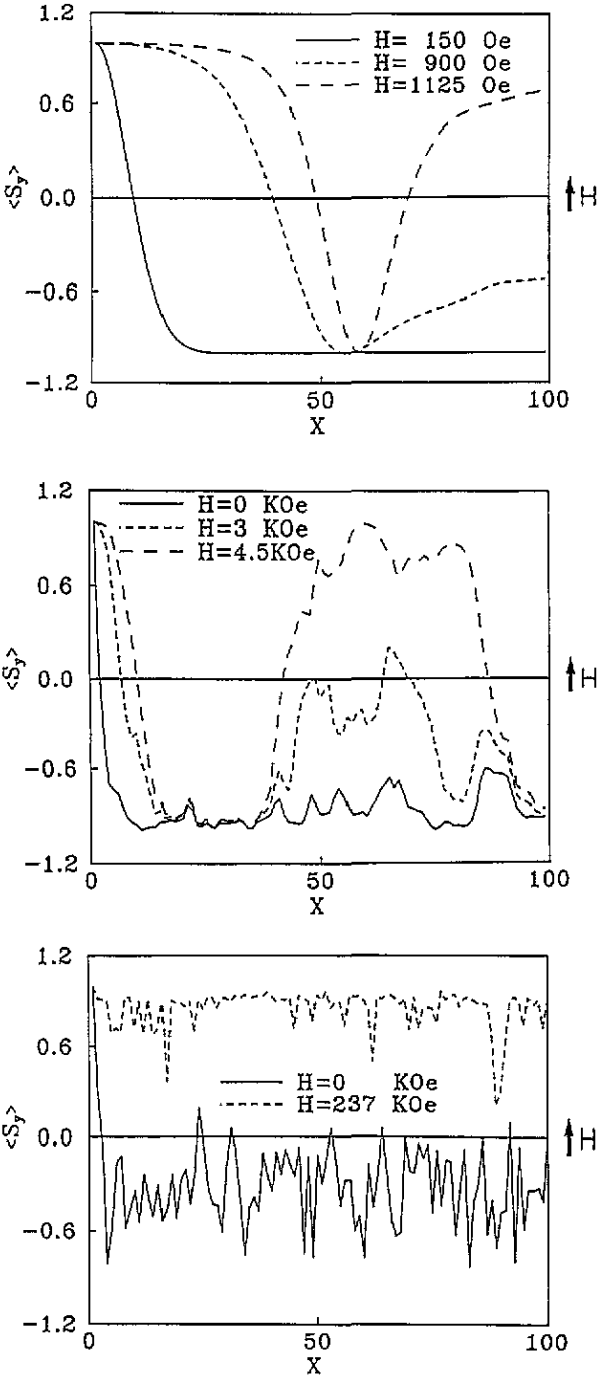

Figure 2. (*a*) The magnetization profile along the length of the sample, for three values of the applied field in the low-anisotropy limit ($D/zJ = 0.1$). A domain wall is initially created at $x = 0$. A topological defect appears at large fields around $x = 55$, which corresponds to a 2π Néel wall. (*b*) The magnetization profile along the length of the sample, for three values of the applied field for $D/zJ = 0.5$. A domain wall is initially created at $x = 0$. (*c*) The magnetization profile along the length of the sample, for two values of the applied field in the high-anisotropy regime ($D/zJ = 2$).

(i) the propagation of the domain wall from the left edge of the sample, where it was created and

(ii) the nucleation of other domains elsewhere in the sample.

The relative role of the two processes depends on the ability of the domain wall to propagate and consequently on the amplitude of the random anisotropy.

In figure 2(a), for $H = 900$ Oe, the domain wall has propagated from the abscissa $x = 9$ to $x = 40$ but, at the same time, the magnetization has started to rotate at the opposite edge of the sample (between $x = 60$ and 100). This rotation is equivalent to the nucleation of a new domain at this opposite edge. When the field is further increased, the initial domain wall continues to propagate and the magnetization in the newly created domain continues to rotate towards the field direction. In between, at abscissa $x = 60$, a singularity in the magnetization profile is observed. This is a linear topologic defect characteristic of XY spins in which the magnetization rotates by 2π. Such linear defects have already been described by Dieny and Barbara [21]. When the field is increased they shrink progressively and their width varies proportionally to $\sqrt{J/H}$. At very large critical fields, they collapse by nucleation of a vortex–antivortex pair and by a further motion of these vortices in opposite directions along the defect.

In the intermediate-anisotropy case (figure 2(b)) the propagation of the domain wall from the left-hand edge of the sample is much less effective than in the former case. Between $H = 0$ kOe and $H = 4.5$ kOe, the domain wall has propagated from abscissa $x = 3$ to $x = 11$. Meanwhile, a domain has been nucleated between $x = 50$ and $x = 80$. In this case the nucleation contributes more than propagation to the inversion process of the magnetization. The random anisotropy indeed induces local energy barriers, which prevent the propagation of the domain walls. These barriers constitute pinning centres for the walls.

In the large-anisotropy case, there is no propagation of the domain walls. The reversal of the magnetization is nucleated everywhere in the system. The propagation mechanism is not operative at all in this case.

In summary, figure 2 illustrates the competition between the propagation of domain walls and the nucleation of new domains in the magnetization reversal processes in random anisotropy systems. The weaker the random anisotropy, the easier the propagation of the domain walls, and therefore the propagation mechanism is preponderant.

The magnetization curves associated with these magnetization processes are plotted in figure 3 for a range of fields from zero to the coercive field of the system. These curves were obtained starting from the same initial spin configuration as in the domain wall motion simulations. Then, the magnetic field was increased until the magnetization vanished (and the magnetic field was equal to the coercive field). As shown in figure 3(a), in the low-anisotropy case, a rather smooth increase in the magnetization is observed with a few irregularities due to the presence of some energy barriers caused by the random anisotropy. Because of the low-amplitude anisotropy, the magnetization has a coherent behaviour over rather a large length scale. This length scale can be estimated by using Imry–Ma phenomenological calculations ([7] and see below), which give a value of $L = zJ/D$ in two dimensions. For $D/zJ = 0.1$ (figure 3(a)) this length scale has the value of 10 lattice constants so the irregularities of the random anisotropy field are smeared out by averaging over this large scale. This leads to the smooth magnetization variation observed.

When the amplitude of the random anisotropy is increased (figure 3(b) and (c)), more and more discontinuities appear, which are analogous to the Barkausen jumps known in ferromagnetic materials. The larger the anisotropy, the larger the number of these jumps and the smaller their amplitude. This feature is related to the decreasing size of the Imry–Ma domains as the anisotropy is increased.

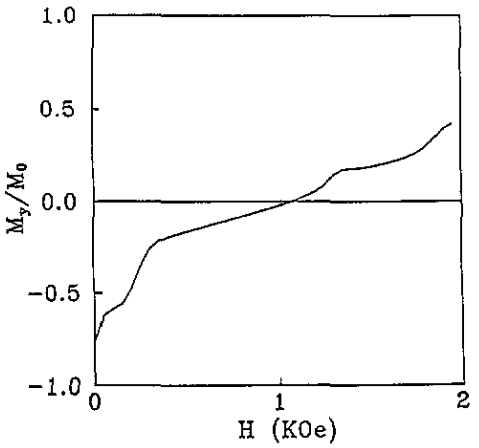

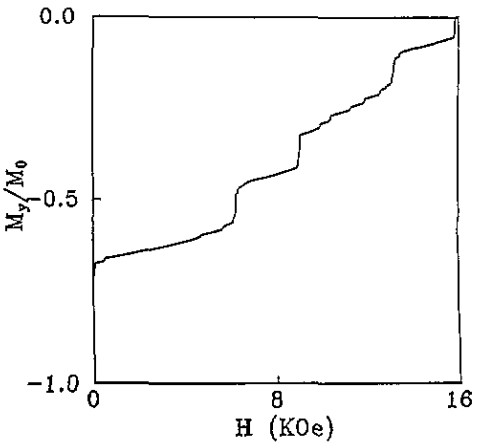

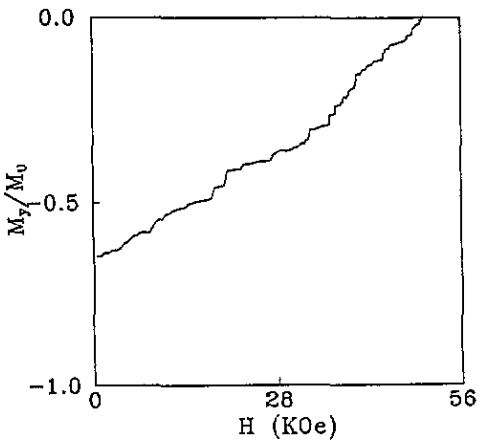

Figure 3. (*a*) Part of the magnetization curve in the low-anisotropy regime ($D/zJ = 0.1$). (*b*) Part of the magnetization curve for $D/zJ = 0.5$. The small discontinuities observed are due to the irreversible motion of domain walls. (*c*) Part of the magnetization curve in the high-anisotropy regime ($D/zJ = 2$).

4. The coercive field at zero temperature

Figure 4 (full circles) shows the variation of the coercive field as a function of the ratio D/zJ at zero temperature assuming that the spins are not able to overcome the energy barriers (non-tunnelling simulations). In the same figure (open circles) the dependence of the coercive field on the ratio D/zJ at zero temperature is shown, assuming that the spins are able to cross the energy barriers due to a tunnelling process, as in the calculations performed by Alben *et al* [10] and Saslow and Koon [12] (tunnelling simulations). These data were obtained by progressively decreasing the magnetic field (applied in the Y direction) from the positive saturation field value $H = H_{sat}$ to decreasing negative fields. In this figure (full circles), two regimes can be distinguished. In the high-anisotropy regime, the coercive field increases linearly with the ratio D/zJ. At $D/zJ = 0.5$, there is a crossover to a new regime, where the coercive field shows a power law behaviour in D/zJ (inset of figure 4). The anisotropy value at which the crossover occurs can be estimated by using Imry–Ma arguments. Indeed, the coercive field of a random anisotropy system is related to the height of the energy barriers due to the random anisotropy. The reversal of the magnetization occurring at $H = H_c$ takes place when most of the spins are able to overcome these energy barriers. On the other hand, the magnetization behaves coherently in a length scale of the order of the Imry–Ma domain size, L. The resulting anisotropy energy for the whole domain is given by $E_{anisotropy} \sim DN^{1/2}$ where $N = L^2$ is the number of spins in the Imry–Ma domains; in our case $E_{anisotropy} \sim DL$. Following the Imry–Ma argument, this energy

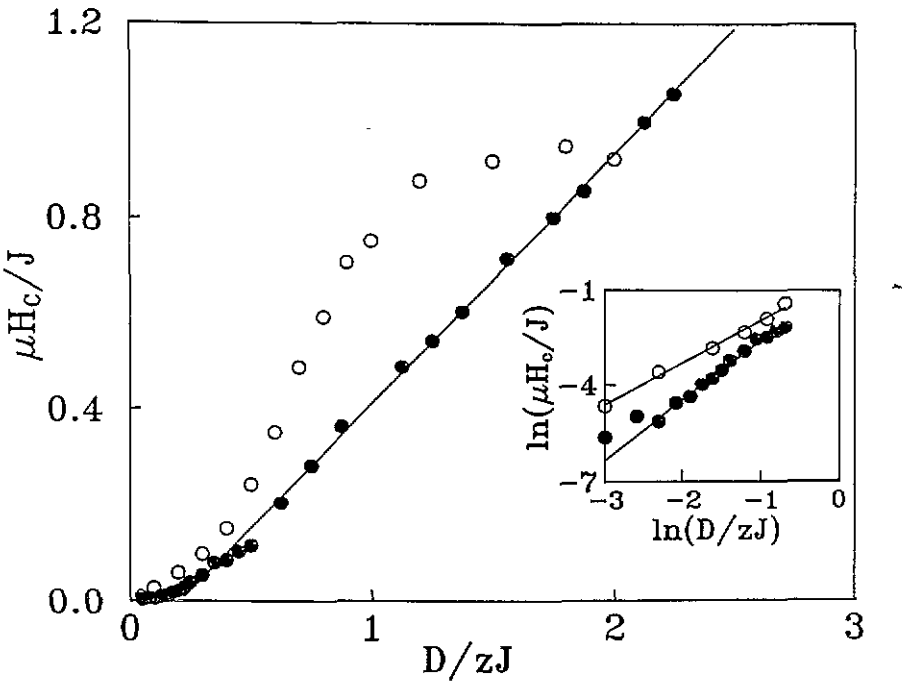

Figure 4. The dependence of the coercive field on the anisotropy strength at zero temperature. The open circles correspond to the tunnelling simulations while the full circles correspond to the non-tunnelling simulations (see the text). In the inset, the low-anisotropy regime is shown in log–log scale. The lines correspond to the best linear fits obtained from the corresponding data.

is balanced by the exchange energy required to form a domain wall between two adjacent Imry–Ma domains. The width of this wall is comparable to the domain size L and the related exchange energy is given by [7] $E_{\text{exchange}} \sim zJ(\pi/L)^2L^2 \sim zJ$. The size L of the Imry–Ma domains is determined by $DL \sim zJ$, i.e. $L \sim zJ/D$.

The height of the anisotropy barriers is thus given by $E_{\text{anisotropy}} \sim DL \sim D(zJ/D) \sim zJ$. This energy barrier may be compared with the Zeeman energy of an Imry–Ma domain at the coercive field, $MH_c \sim E_{\text{anisotropy}}$, where $M = \mu L^2$ is the magnetic moment of a domain and μ is the magnetic moment of one spin of the system. This finally leads to $H_C \sim D^2/zJ$.

The results agree qualitatively with the theoretical predictions of Imry and Ma [7]. In the inset of figure 4, the low-anisotropy region is shown in log–log scale for the simulations, assuming no tunnelling of the energy barriers (full circles) and for the simulations assuming tunnelling of the energy barriers (open circles). The fitting to a power law is good and gives an exponent of 1.9 ± 0.1 in the case of no tunnelling of the energy barriers (full circles) and 1.4 ± 0.1 in the case of tunnelling of the energy barriers (open circles). The quantitative difference observed in the value of the exponent may originate from two sources, firstly, the intrinsic error in the data, due to the simulation method, and secondly, the error in the numerical estimation of the exponent. The error associated with the simulation method is basically due to the field step used to obtain the hysteresis loops, from which the coercive field was calculated. In the present simulation, the field step has been chosen to minimize the non-equilibrium effects, so it cannot be decreased. The error in the numerical estimation

of the exponent originates from the intrinsic statistical errors of the points used in the linear regression procedure. Both sources of error may be reduced by averaging over different ensembles of random anisotropy axes to compensate the statistical fluctuations between the ensembles and by increasing the system size. As the aim of the work was to obtain qualitative information on the magnetization process, the average over different ensembles of random anisotropy axes was not carried out, to keep the computing time within reasonable margins. In spite of the above-mentioned sources of error, it is worth noting that the value of the exponent of the power law is closer to the theoretical one in the case on non-tunnelling simulations. This may be because the Imry–Ma arguments are classical, and do not include any mechanism of tunnelling of the energy barriers, so they are closer to the assumptions made in the non-tunnelling simulations. Below $D/zJ < 0.1$ a deviation from the power law is observed due to the finite size of the system. In this case, the magnetic domains are larger than the simulated system.

The onset of the high-anisotropy regime occurs when the characteristic domain size, L, is approximately equal to two or three atomic distances. At this point, the magnetic correlations due to the exchange interaction are lost, so the spins behave independently, as an assembly of very small independent clusters, and the coercive field grows linearly with the ratio D/zJ. The slope of the curve is related to the number of spins in the small clusters. To study this behaviour, we have used the Stoner–Wohlfarth model [24] for a set of independent particles with cubic anisotropy. The behaviour of the coercive field predicted by Stoner and Wohlfarth is

$$H_c = 2K/M_{sat} \tag{2}$$

where K is the cubic anisotropy constant and M_{sat} is the saturation magnetization of the Imry–Ma domain. In our case, the randomness of anisotropy direction can be taken into account using the Néel expression for the coercive field [25]

$$H_c = 0.64K/M_{sat}. \tag{3}$$

The saturation magnetization can be expressed as $N\mu$ where μ is the magnetic moment of one spin and N is the mean number of spins in the magnetic clusters. From the calculated slope of the full-circle curve (non-tunnelling simulations), we can obtain the average number N of spins in each cluster. The value obtained is between one and two spins, which is in good agreement with the spin configurations shown in figure 1(*b*) and (*c*). In the high-anisotropy regime, the Imry–Ma arguments, which are derived from a continuous approximation, are no longer valid, the characteristic length L becomes smaller than the lattice constant and the discretization effects become critical.

Our results are in qualitative agreement with the mean-field predictions made by Callen *et al* [9] and Patterson *et al* [11] and agree with the results obtained by Alben *et al* [10] and Saslow and Koon [12] in the low- and intermediate-anisotropy regime. However, in the high-anisotropy regime ($D/zJ > 1$) differences arise. In the present calculation (figure 4, full circles), the coercive field grows linearly as the anisotropy amplitude increases while, in the Alben *et al* [10] calculations, the coercive field grows linearly up to $D/zJ = 2$, and reaches a maximum value around $D/zJ = 2.6$. For higher values of the ratio D/zJ, the coercive field decreases to an asymptotic value close to $g\mu_B H_c/J = 2$. On the other hand, in the Saslow–Koon [12] numerical simulations, the coercive field increases with the ratio D/zJ and reaches a constant value close to $1.3J$ in the high-anisotropy regime. In our opinion, these discrepancies may be related to the assumption made by Alben *et al*

[10] and Saslow and Koon [12] about the ability of the spins to overcome the energy barriers. They assume that there is a tunnelling probability equal to one, i.e. at zero temperature all the energy barriers can be overcome by the tunnel effect; while in the present calculation the spins are not allowed to pass any energy barrier (steepest-descent algorithm). To understand this difference better, the dependence of the coercive field on the ratio D/zJ at zero temperature has been calculated assuming that the spins can always overcome the energy barriers and reach the absolute minimum of energy. The results are also shown in figure 4 (open circles). Although the shape of the curve in the low-anisotropy regime is slightly different from the full-circle curve, the power law region and the linear region (with different slope) are still present. However, in the high-anisotropy limit, the coercive field reaches an asymptotic value close to J/μ_B. This behaviour can be understood as follows. In the low-anisotropy regime, each spin has only one energy minimum in its local field. Then, both curves are approximately the same. When D/zJ is close to 0.5, a secondary minimum appears and then the differences arise. In the case of figure 4 (full circles), the spins are not allowed to overcome the energy barriers, so the higher the anisotropy, the higher the energy barriers and the higher the coercive field needed to overcome these energy barriers. However, if all the energy barriers are overcome (open circles), the height of the energy barriers (which is proportional to the anisotropy amplitude) is no longer important and the coercive field reaches a constant value J/μ_B.

In conclusion, the difference in the behaviour of the coercive field in the high-anisotropy regime may be due to the way that metastability is taken into account. If the spins are allowed to overcome all the energy barriers, as in [10] and [12], the zero-temperature coercive field reaches an asymptotic value close to the exchange field because all the energy barriers are overcome and the system behaves, in the high-anisotropy regime, as if all the spins of the system were in the deepest energy minimum. On the other hand, if the spins are not able to overcome all the energy barriers, the system shows more metastability, since local energy minima are relevant and the spins are forced to pass through the intermediate metastable states. In consequence, the coercive field increases when the anisotropy increases. The assumption made by Alben *et al* [10] and Saslow and Koon [12] about the overcoming of the energy barriers is equivalent to introducing a quantum tunnelling transition probability between the energy minima that disregards the influence of the metastability in the magnetic behaviour of the system. Although this quantum tunnelling transition probability might be important at zero temperature we think that the effect of the metastability is more important for the explanation of the magnetic behaviour of these systems and should be taken into account.

5. The thermal behaviour of the coercive field

Regarding the thermal behaviour of the coercive field, numerical simulations were performed using the classical Monte Carlo method [23] starting from saturation and decreasing the magnetic field (applied in the Y direction) in steps of 2000 Oe. Between each field variation the system was equilibrated during 1500 MCS. The results are shown in figure 5 for three different values of the D/zJ ratio. Some experiments [13–15] suggested an exponential decay of the coercive field as the temperature increases. We have attempted to fit our data to the exponential law $H_c(D/zJ, T) = H_c(D/zJ, 0)e^{-\alpha T}$ and the results are also given in figure 5. The fits were in good agreement with the data, so the dependence of α on the ratio D/zJ was estimated. In figure 6 the results for $\alpha(D/zJ)$ are shown. In spite of the error bars (associated with the field steps) the exponent α increases as D/zJ increases

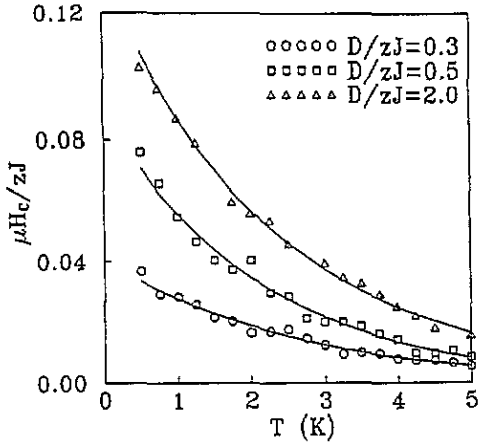

Figure 5. The thermal variation of the coercive field for three different values of the anisotropy amplitude. The solid lines represent the best fit of the data to an exponential law.

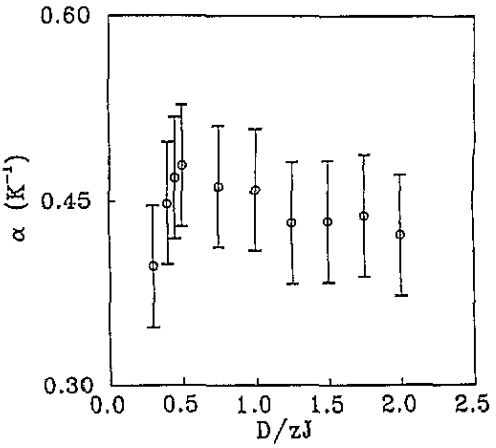

Figure 6. The dependence of the decay rate α on the ratio D/zJ derived from the fits of the thermal variation of the coercive field to an exponential decay.

for anisotropy strength lower than 0.5 where the exponent α reaches the maximum value. Then, for higher values of the ratio D/zJ, the exponent α decreases smoothly as D/zJ increases. This dependence of α on the ratio D/zJ can be understood as follows. The coercive field measures the difficulty of reversing the magnetization of the whole system. On the other hand, the height of the energy barriers, which prevents the reversal of the magnetization, is related to the amplitude of the random anisotropy. Relative to this height, the thermal activation plays a different role for low anisotropy and for high anisotropy. In the low-anisotropy regime, the inversion process occurs by rotation of the magnetization in the clusters, as it has been shown in section 2. As the anisotropy strength increases the characteristic cluster size decreases and the inversion is easier, because it involves fewer spins. Then the thermal activation facilitates the change of orientation of the magnetic moments. In consequence, the coercive field decreases faster for increasing D/zJ so the exponent α becomes higher. In the high-anisotropy regime, the inversion process involves single spin inversions, because the magnetization of the system has been broken by the random anisotropy into very small clusters of two or three spins. Then, as the anisotropy strength is increased the pinning effect caused by the random anisotropy becomes critical and hampers the magnetization reversal. As a result, the coercive field decreases slowly as the temperature increases and the exponent α decreases. At $D/zJ = 0.5$, the rate α reaches a maximum, which corresponds to a crossover from the low-anisotropy regime to the high-anisotropy regime. This result can also be interpreted using the micromagnetic calculation performed by Gaunt [26], who studied the thermal variation of the coercive field for a magnetic material with a random array of defects, each of which has a phenomenological interaction potential with the domain walls. As a result, Gaunt found that the stronger this potential is the slower is the decrease in the coercive field as the temperature is increased.

Acknowledgments

This work was made possible in part by a grant from the CIRIT (Comisió Interdeparamental de Recerca i Innovació Tecnològica) AIRE-92. We are grateful to the Laboratoire Louis Néel

for their hospitality while this work was in progress. Some of the calculations were carried out on an IBM 3090/600 computer at CESCA (Centre de Supercomputació de Catalunya).

References

[1] Moorjani K and Coey J M D 1984 *Magnetic Glasses* (Amsterdam: Elsevier)
[2] Rhyne J J, Schelleng J H and Koon N C 1974 *Phys. Rev.* B **10** 4672
[3] Sellmyer D J and Nafis S 1986 *Phys. Rev. Lett.* **57** 1173
[4] Buschow K H J 1991 *Handbook of Magnetic Materials* vol 6 (Amsterdam: North-Holland–Elsevier)
Wohlfarth E P 1980 *Ferromagnetic Materials* vol 2 (Amsterdam: North-Holland–Elsevier)
[5] Harris R, Plischke M, Zuckermann M J 1973 *Phys. Rev. Lett.* **31** 160
[6] Harris R, Zobin D 1977 *J. Phys. F: Met. Phys.* **7** 337
[7] Imry Y and Ma S K 1975 *Phys. Rev. Lett.* **35** 1399
[8] Aharony A and Pytte E 1980 *Phys. Rev. Lett.* **45** 1538; 1983 *Phys. Rev.* B **27** 5872
[9] Callen E, Liu Y I and Cullen J R 1977 *Phys. Rev.* B **16** 263
[10] Alben R, Becker J and Chi M C 1978 *J. Appl. Phys.* **49** 1653
[11] Patterson J D, Gruzalski G R and Sellmeyer D J 1978 *Phys. Rev.* B **18** 1377
[12] Saslow W M and Koon N C 1994 *Phys. Rev.* B **49** 3386
[13] Read D A, Moyo T and Hallan G C 1984 *J. Magn. Magn. Mater.* **44** 279
[14] Buschow K J and Kraan A M 1981 *J. Magn. Magn. Mater.* **22** 220
[15] Arnaudas J I, del Moral A, de la Fuente C and de Groot P A J 1993 *Phys. Rev.* B **47** 11 924
[16] Jayaprakash C and Kirkpatrick C 1980 *Phys. Rev.* B **21** 4072
[17] Denholm D R and Sluckin T J 1993 *Phys. Rev.* B **48** 901
[18] Cresswell A and Paul D I 1990 *J. Appl. Phys.* **67** 398
[19] Wohlfarth E P 1984 *J. Phys. F: Met. Phys.* **14** L155
[20] Chudnovsky E M and Serota R A 1982 *Phys. Rev.* B **26** 2697
Chudnovsky E M, Saslow W M and Serota R A 1986 *Phys. Rev.* B **33** 251
[21] Dieny B and Barbara B 1990 *Phys. Rev.* B **41** 11 549
[22] Press W H, Flannery B P, Teukolsky S A and Vetterling W T 1988 *Numerical Recipes in Fortran* (Cambridge: Cambridge University Press)
[23] Binder K 1979 *Monte Carlo Methods in Statistical Physics* vol 7 (Berlin: Springer)
[24] Stoner E C and Wohlfarth E P 1948 *Phil. Trans. R. Soc.* A **240** 599
[25] Néel L 1947 *C. R. Acad. Sci., Paris* **224** 1488
[26] Gaunt P 1983 *Phil. Mag.* B **48** 261